Molecular Therapy
Nucleic Acids
Original Article

Suppression of endothelial miR-22 mediates non-small cell lung cancer cell-induced angiogenesis

Yuan Gu,[1] Gianni Pais,[1] Vivien Becker,[1] Christina Körbel,[1] Emmanuel Ampofo,[1] Elke Ebert,[2] Johannes Hohneck,[2] Nicole Ludwig,[3] Eckart Meese,[3] Rainer M. Bohle,[2] Yingjun Zhao,[4] Michael D. Menger,[1] and Matthias W. Laschke[1]

[1]Institute for Clinical and Experimental Surgery, Saarland University, 66421 Homburg/Saar, Germany; [2]Institute of Pathology, Saarland University, 66421 Homburg/Saar, Germany; [3]Institute of Human Genetics, Saarland University, 66421 Homburg/Saar, Germany; [4]Fudan University Shanghai Cancer Center and Institutes of Biomedical Sciences, Department of Oncology, Shanghai Medical College, Fudan University, Shanghai 200032, China

MicroRNAs (miRNAs) expressed in endothelial cells (ECs) are powerful regulators of angiogenesis, which is essential for tumor growth and metastasis. Here, we demonstrated that miR-22 is preferentially and highly expressed in ECs, while its endothelial level is significantly downregulated in human non-small cell lung cancer (NSCLC) tissues when compared to matched nontumor lung tissues. This reduction of endothelial miR-22 is possibly induced by NSCLC cell-secreted interleukin-1β and subsequently activated transcription factor nuclear factor-κB. Endothelial miR-22 functions as a potent angiogenesis inhibitor that inhibits all of the key angiogenic activities of ECs and consequently NSCLC growth through directly targeting sirtuin 1 and fibroblast growth factor receptor 1 in ECs, leading to inactivation of AKT/mammalian target of rapamycin signaling. These findings provide insight into the molecular mechanisms of NSCLC angiogenesis and indicate that endothelial miR-22 represents a potential target for the future antiangiogenic treatment of NSCLC.

INTRODUCTION

Angiogenesis, i.e., the formation of new blood vessels from preexisting ones, is essential for tumor growth and metastasis. Accordingly, excessive angiogenesis is a poor prognostic indicator for the aggressiveness of different cancer types such as non-small cell lung cancer (NSCLC).[1] Tumor angiogenesis is tightly regulated by the balance between pro- and antiangiogenic factors, which involves the dynamic communication between tumor cells and endothelial cells (ECs). Tumor cells are capable of releasing different proangiogenic factors such as vascular endothelial growth factor (VEGF), basic fibroblast growth factor (bFGF, FGF2), epidermal growth factor (EGF), tumor necrosis factor (TNF)-α, interleukin (IL)-1β, IL-6, and IL-8.[2,3] The binding of these factors to their receptors located on ECs activates pivotal downstream angiogenesis-related signaling pathways such as phosphoinositide 3 kinase (PI3K)/v-akt murine thymoma viral oncogene homolog (AKT)/mammalian target of rapamycin (mTOR) signaling.[4] Consequently, ECs are stimulated to degrade their basement membrane, proliferate, migrate toward tumor cells, and interconnect with each other to form new microvascular networks.[2,4]

Previous studies have shown that sirtuin (SIRT) 1 plays a crucial role in the regulation of angiogenesis.[5] SIRT1 is a prototype member of the sirtuin family of nicotinamide adenine dinucleotide-dependent class III histone deacetylases. Loss of SIRT1 results in a significant reduction of EC sprouting and branching activity.[5] Moreover, endothelial SIRT1 deletion impairs angiogenesis within ischemic hindlimbs and the kidney.[5,6] The proangiogenic effect of SIRT1 is most probably mediated by some of its substrates. In fact, it has been reported that SIRT1 deacetylates AKT, which binds to phosphatidylinositol (3,4,5)-triphosphate, leading to the activation of the AKT/mTOR pathway.[7] In addition, SIRT1 deacetylates the forkhead transcription factor FOXO1 and thus suppresses its antiangiogenic activity.[5] SIRT1 can also promote the phosphorylation of AKT by upregulating the transcription of Rictor, a component of mechanistic target of rapamycin complex 2.[8]

MicroRNAs (miRNAs) are short (~22 nucleotides), endogenous, noncoding RNAs that modulate gene expression primarily through binding to the 3′ untranslated region (UTR) of messenger RNA (mRNA), leading to mRNA degradation and translation inhibition.[9] In the last decade, accumulating evidence has suggested miRNAs as powerful regulators of angiogenesis. Furthermore, miRNA deregulation has been linked to tumor development and progression. Of interest, alterations of miR-22 expression within different human body fluids and tumor tissues are considered to be of great significance for the diagnosis, surveillance, and prognosis of multiple types of cancer such as NSCLC.[10] miR-22, also called miR-22-3p, is located on chromosome 17p13 and highly conserved among metazoans.[11] It has been reported to be expressed in different types of ECs.[12] However, its role in regulating tumor angiogenesis remains elusive.

Received 11 May 2021; accepted 1 October 2021;
https://doi.org/10.1016/j.omtn.2021.10.003.

Correspondence: Yuan Gu, Institute for Clinical and Experimental Surgery, Saarland University, 66421 Homburg/Saar, Germany.
E-mail: yuan.gu@uks.eu

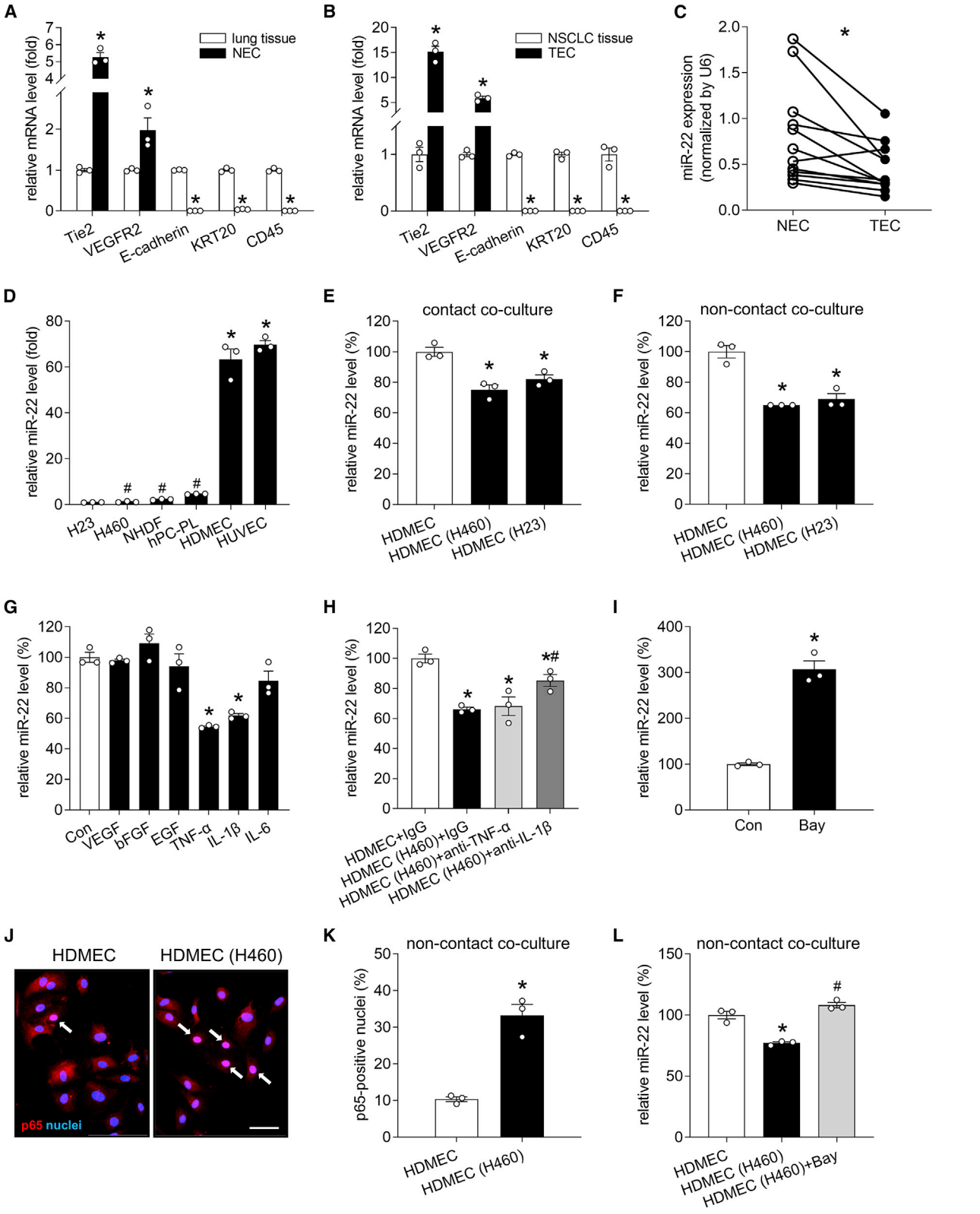

(legend on next page)

In the present study, we analyzed the regulation of endothelial miR-22 by NSCLC cells. We then systematically investigated the function of miR-22 in basic angiogenic processes, including EC proliferation, migration, and tube formation. The observed antiangiogenic action of miR-22 was further confirmed in an *ex vivo* mouse aortic ring assay and an *in vivo* Matrigel plug assay. In addition, we studied the effects of endothelial miR-22 on NSCLC angiogenesis and growth in a mouse flank tumor model. Finally, mechanistic analyses identified *SIRT1* and FGF receptor (*FGFR*)*1* as functional targets of miR-22 in ECs.

RESULTS

Endothelial miR-22 is downregulated in human NSCLC tissues

To compare the expression of miR-22 in tumor endothelial cells (TECs) and normal endothelial cells (NECs), ECs lining the blood vessels in tumor tissues and matched adjacent nontumor lung tissues from 12 patients with lung adenocarcinoma (Table S1) were retrieved by means of laser capture microdissection (LCM). A high enrichment of ECs by LCM was confirmed by a markedly higher expression of the EC markers Tie2 and VEGF receptor 2 (VEGFR2) as well as a lower expression of the epithelial markers E-cadherin and keratin 20 (KRT20) and the leukocyte marker CD45 in microdissected NECs and TECs when compared to that in lung tissue and NSCLC tissue, respectively (Figures 1A and 1B). These isolated ECs were processed for real-time PCR analysis to evaluate the expression level of miR-22. By this, we could demonstrate that miR-22 is significantly downregulated in ECs isolated from NSCLC tissues when compared to those isolated from matched nontumor lung tissues (Figure 1C). We also analyzed the correlation between endothelial miR-22 expression and clinical characteristics of NSCLC patients. According to the mean value (0.46) of the expression level of endothelial miR-22, the NSCLC patients were divided into a low miR-22 group (n = 7) and a high miR-22 group (n = 5). Subsequently, clinical characteristics, including tumor size, tumor grade, lymph node metastasis, lymphatic invasion, and vascular invasion, were compared between the two groups. We found that a low expression of endothelial miR-22 may be associated with vascular invasion of NSCLC (Table S2).

Of note, miR-22 was found to be preferentially and highly expressed in both types of analyzed ECs, i.e., human dermal microvascular endothelial cells (HDMECs) and human umbilical vein endothelial cells (HUVECs), when compared to NSCLC cells (NCI-H460 and NCI-H23) and other cell types in the tumor microenvironment such as pericytes (human pericytes from placenta [hPC-PLs]) and fibroblasts (normal human dermal fibroblasts [NHDFs]). This indicates a plausible regulatory function of miR-22 in ECs (Figure 1D).

NSCLC cells downregulate miR-22 expression in ECs

Since tumor cells are capable of stimulating the angiogenic activity of ECs by both direct cell-cell contact and paracrine signaling, we next utilized a contact coculture system to investigate how the expression of miR-22 in HDMECs is regulated by NSCLC cells. After 24 h of either culturing HDMECs alone or coculturing them with NCI-H460 or NCI-H23 cells, HDMECs were isolated using CD31 magnetic beads. The purity of isolated HDMECs was approximately 99% and 90% in the HDMEC monoculture and coculture groups, respectively, as assessed by flow cytometry. Real-time PCR assays revealed a 25% and a 18% reduction of miR-22 expression in HDMECs cocultured with NCI-H460 cells and NCI-H23 cells when compared to HDMEC monoculture (Figure 1E). In an additional set of experiments, we cocultured HDMECs with NSCLC cells but without contact between these two cell types in a transwell plate. Interestingly, this noncontact coculture with NCI-H460 cells caused a 35% decrease in the miR-22 expression level of HDMECs (Figure 1F), indicating that soluble factors secreted by the tumor cells contribute to the downregulation of endothelial miR-22. This finding was confirmed by the coculture of HDMECs with NCI-H23 cells, which also significantly reduced the endothelial expression of miR-22 by 31% (Figure 1F).

Figure 1. NSCLC cells downregulate miR-22 expression in ECs

(A) mRNA levels (in fold of lung tissue) of Tie2, VEGFR2, E-cadherin, KRT20, and CD45 in lung tissue from NSCLC patients or retrieved ECs from lung tissue (NECs) by means of LCM, as assessed by real-time PCR (n = 3). (B) mRNA levels (in fold of NSCLC tissue) of Tie2, VEGFR2, E-cadherin, KRT20, and CD45 in NSCLC tissue from patients or retrieved ECs from NSCLC tissue (TECs) by means of LCM, as assessed by real-time PCR (n = 3). (C) Expression level of miR-22 (normalized by U6) in NECs and TECs from NSCLC patients, as assessed by real-time PCR (n = 12). (D) Expression level of miR-22 (in fold of H23) in NCI-H23 cells, NCI-H460 cells, NHDFs, hPC-PLs, HDMECs, and HUVECs, as assessed by real-time PCR (n = 3). (E) Expression level of miR-22 (in % of HDMEC) in isolated HDMECs that were cultured alone (HDMEC) or cocultured in direct contact with NCI-H460 cells [HDMEC (H460)] or NCI-H23 cells [HDMEC (H23)] for 24 h, as assessed by real-time PCR (n = 3). (F) Expression level of miR-22 (in % of HDMEC) in HDMECs that were cultured alone (HDMEC) or cocultured with NCI-H460 cells [HDMEC (H460)] or NCI-H23 cells [HDMEC (H23)] without contact in a transwell plate for 24 h, as assessed by real-time PCR (n = 3). (G) Expression level of miR-22 (in % of Con) in HDMECs that were exposed for 24 h to vehicle (Con), 50 ng/mL of VEGF, 50 ng/mL of bFGF, 100 ng/mL of EGF, 10 ng/mL of TNF-α, 2 ng/mL of IL-1β, or 100 ng/mL of IL-6 in EBM, as assessed by real-time PCR (n = 3). (H) Expression level of miR-22 (in % of HDMEC+IgG) in HDMECs that were cultured alone (HDMEC) or cocultured with NCI-H460 cells [HDMEC (H460)] without contact in a transwell plate in the presence of 5 μg/mL of IgG, anti-TNF-α NAb, or anti-IL-1β NAb for 24 h, as assessed by real-time PCR (n = 3). (I) Expression level of miR-22 (in % of Con) in HDMECs that were treated for 24 h with vehicle (Con) or 1 μM of Bay 11-7082 (Bay), as assessed by real-time PCR (n = 3). (J) Cellular localization of NF-κB in HDMECs that were cultured alone or cocultured with NCI-H460 cells without contact in a transwell plate and stained for p65 (red). Cell nuclei were labeled with Hoechst 33342 (blue). The nuclear translocation of p65 is indicated by arrows. Scale bar, 60 μm. (K) p65-positive nuclei (in % of the total number of nuclei) of HDMECs that were cultured alone (HDMEC) or cocultured with NCI-H460 cells [HDMEC (H460)] without contact in a transwell plate, as assessed by immunocytochemistry (n = 3). (L) Expression level of miR-22 (in % of HDMEC) in HDMECs that were cultured alone (HDMEC) or cocultured with NCI-H460 cells [HDMEC (H460)] without contact in a transwell plate in the absence or presence of 1 μM of Bay 11-7082 (Bay) for 24 h, as assessed by real-time PCR (n = 3). Data are means ± SEM. *$p < 0.05$ versus lung tissue, NSCLC tissue, NEC, H23, HDMEC, or Con; #$p < 0.05$ versus HDMEC (D) or HDMEC (H460) (H and L).

Previous studies reported the ability of NSCLC cells to secrete several well-known proangiogenic factors, including VEGF, bFGF, EGF, TNF-α, IL-1β, and IL-6.[13–16] To investigate whether any of these factors mediates the NSCLC cell-induced reduction of endothelial miR-22, HDMECs were stimulated with each factor for 24 h. Real-time PCR analyses revealed that the expression of miR-22 is significantly suppressed by TNF-α and IL-1β but is not affected by VEGF, bFGF, EGF, and IL-6 stimulation (Figure 1G). Of interest, blockade of IL-1β, but not TNF-α, with neutralizing antibody (NAb) significantly counteracted the downregulation of miR-22 in HDMECs induced by noncontact coculture with NCI-H460 cells (Figure 1H). This finding suggests that NSCLC cells reduce endothelial miR-22 expression at least partially through secreting IL-1β. Given the fact that IL-1β is an upstream inducer of nuclear factor (NF)-κB, which promotes or represses the transcription of a broad spectrum of genes and miRNAs,[17,18] we then investigated whether NF-κB inhibits the transcription of miR-22 in ECs. For this purpose, HDMECs were exposed to the NF-κB inhibitor Bay 11-7082 for 24 h. This resulted in a 2-fold increase of miR-22 expression when compared to vehicle-treated controls (Figure 1I), indicating that this miRNA is transcriptionally repressed by NF-κB.

To investigate whether NF-κB mediates the downregulation of endothelial miR-22 induced by NSCLC cells, we assessed the activation status of NF-κB in HDMECs cultured alone or cocultured with NCI-H460 cells without contact. By means of immunofluorescence, we demonstrated that the nuclear translocation of p65, a main subunit of NF-κB, is significantly enhanced in HDMECs cocultured with tumor cells (Figures 1J and 1K). Importantly, inhibition of NF-κB signaling with Bay 11-7082 completely reversed the reduction of endothelial miR-22 induced by noncontact coculture with NCI-H460 cells (Figure 1L).

miR-22 inhibits the angiogenic activity of ECs

To study the function of miR-22 in regulating EC angiogenic activity, we transfected HDMECs with miR-22 mimic (miR-22m) and miR-22 inhibitor (miR-22i) to up- and downregulate the intracellular level of this miRNA, respectively. Cells transfected with the negative control of mimic (NCm) or the negative control of inhibitor (NCi) served as controls. To assess the success of these manipulations, the transfection efficiencies of miR-22m (5 nM) and miR-22i (100 nM) were evaluated by real-time PCR assays. As shown in Figures S1A and S1B, transfection with miR-22m significantly upregulated the intracellular miR-22 level by 64.8-fold, while miR-22i markedly reduced miR-22 expression by 97.8%.

At first, water-soluble tetrazolium (WST)-1 assays were performed to assess the viability of ECs. Transfection with miR-22m significantly reduced the viability of HDMECs after 48 h of incubation (Figure 2A). This inhibitory effect of miR-22m was detectable for at least 10 days (Figure S1C). In contrast, an increased viability rate was observed in miR-22i-transfected ECs (Figure 2B). The effect of miR-22 on EC proliferation was further analyzed by flow cytometry assessing the cell cycle distribution of transfected HDMECs. The S-phase cell population was significantly increased in miR-22m-transfected HDMECs when compared to NCm-transfected controls (Figures S2A and S2B). This was associated with an increase in the number of sub-G1-phase cells (Figures S2A and S2C). These results suggest that miR-22 inhibits EC proliferation and induces apoptosis by blocking the cells in the S phase.

To investigate the function of miR-22 in regulating EC motility, scratch wound healing assays and transwell migration assays were performed. Transfection of HDMECs with miR-22m markedly delayed the healing of scratched wounds (Figures 2C and 2E) and reduced the number of transwell migrated cells by 34% (Figures S3A and S3B). In contrast, transfection of HDMECs with miR-22i significantly promoted wound closure (Figures 2D and 2F) and enhanced cell migration by 42% (Figures S3C and S3D).

In addition, we performed tube formation assays to investigate the function of miR-22 in regulating the tube-forming activity of HDMECs. Transfection with miR-22m markedly reduced the number of newly developed tube meshes by 76% when compared to NCm-transfected controls (Figures 2G and 2H). In contrast, miR-22i significantly augmented EC tube formation by 64% (Figures 2I and 2J).

Endothelial miR-22 suppresses angiogenesis *ex vivo* and *in vivo*

To elucidate whether miR-22 is involved in endothelial sprouting, we performed an *ex vivo* mouse aortic ring assay. We found that the area of vascular sprouting from aortic rings is significantly decreased by transfection with miR-22m (Figures 3A and 3B) and significantly increased by transfection with miR-22i (Figures 3C and 3D).

To confirm our *in vitro* findings, we performed an *in vivo* Matrigel plug assay. Matrigel plugs containing miR-22m-transfected HDMECs exhibited a 58% reduction of the microvessel density 7 days after implantation when compared to those containing NCm-transfected controls (Figures 3E and 3F). In contrast, plugs containing miR-22i-transfected cells presented with a 42% higher microvessel density than plugs containing NCi-transfected cells (Figures 3G and 3H).

Endothelial miR-22 inhibits tumor angiogenesis and growth

The findings above demonstrated that (1) NSCLC cells downregulate the expression level of miR-22 in ECs and (2) miR-22 acts as a potent angiogenesis inhibitor. Hence, we assumed that tumor cells stimulate angiogenesis at least partially through suppressing endothelial miR-22 expression. To verify this hypothesis, we established an *in vivo* tumor cell-EC communication model by injecting NCI-H460 cells together with NCm- or miR-22m-transfected HDMECs into the flanks of nonobese diabetic-severe combined immunodeficiency (NOD-SCID) mice. Digital caliper measurements and high-resolution ultrasound imaging were performed to assess the volume of the newly developing tumors. We found that transfection of HDMECs with miR-22m significantly inhibits NCI-H460 tumor development between days 7 to 14 when compared to NCm-

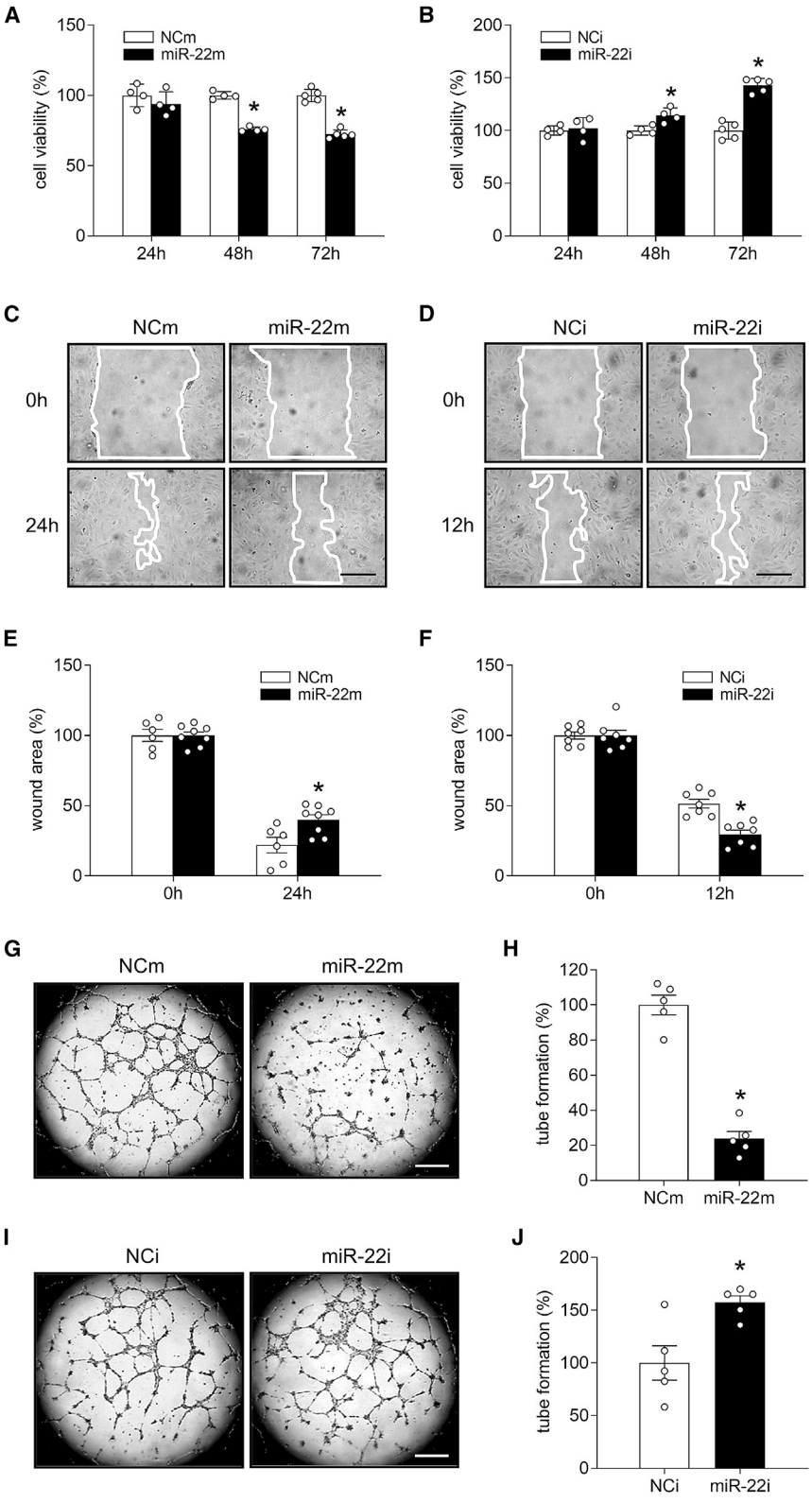

Figure 2. miR-22 inhibits HDMEC viability, migration, and tube formation

(A and B) Viability (in % of NCm or NCi) of HDMECs transfected with miR-22m (A), miR-22i (B), or corresponding scrambled NCm (A) and NCi (B), as assessed by the WST-1 assay (n = 4 to 5). After transfection, the cells were reseeded in 96-well plates and cultured for 24, 48, or 72 h. (C and D) Phase-contrast microscopic images of HDMECs at 0, 12, or 24 h after scratching. The cells were transfected with miR-22m (C), miR-22i (D), or corresponding scrambled NCm (C) and NCi (D). White lines indicate the scratched wound area. Scale bars, 190 μm. (E and F) Wound area (in % of 0 h) created by scratching the monolayer of HDMECs transfected with miR-22m (E), miR-22i (F), or corresponding scrambled NCm (E) and NCi (F), as assessed by the scratch wound healing assay (n = 6 to 8). (G and I) Phase-contrast microscopic images of tube-forming HDMECs. The cells were transfected with miR-22m (G), miR-22i (I), or corresponding scrambled NCm (G) and NCi (I). Scale bars, 550 μm. (H and J) Tube formation (in % of NCm or NCi) of HDMECs transfected with miR-22m (H), miR-22i (J), or corresponding scrambled NCm (H) and NCi (J), as assessed by the tube formation assay (n = 5). Data are means ± SEM. *$p < 0.05$ versus NCm or NCi. See also Figures S1–S3.

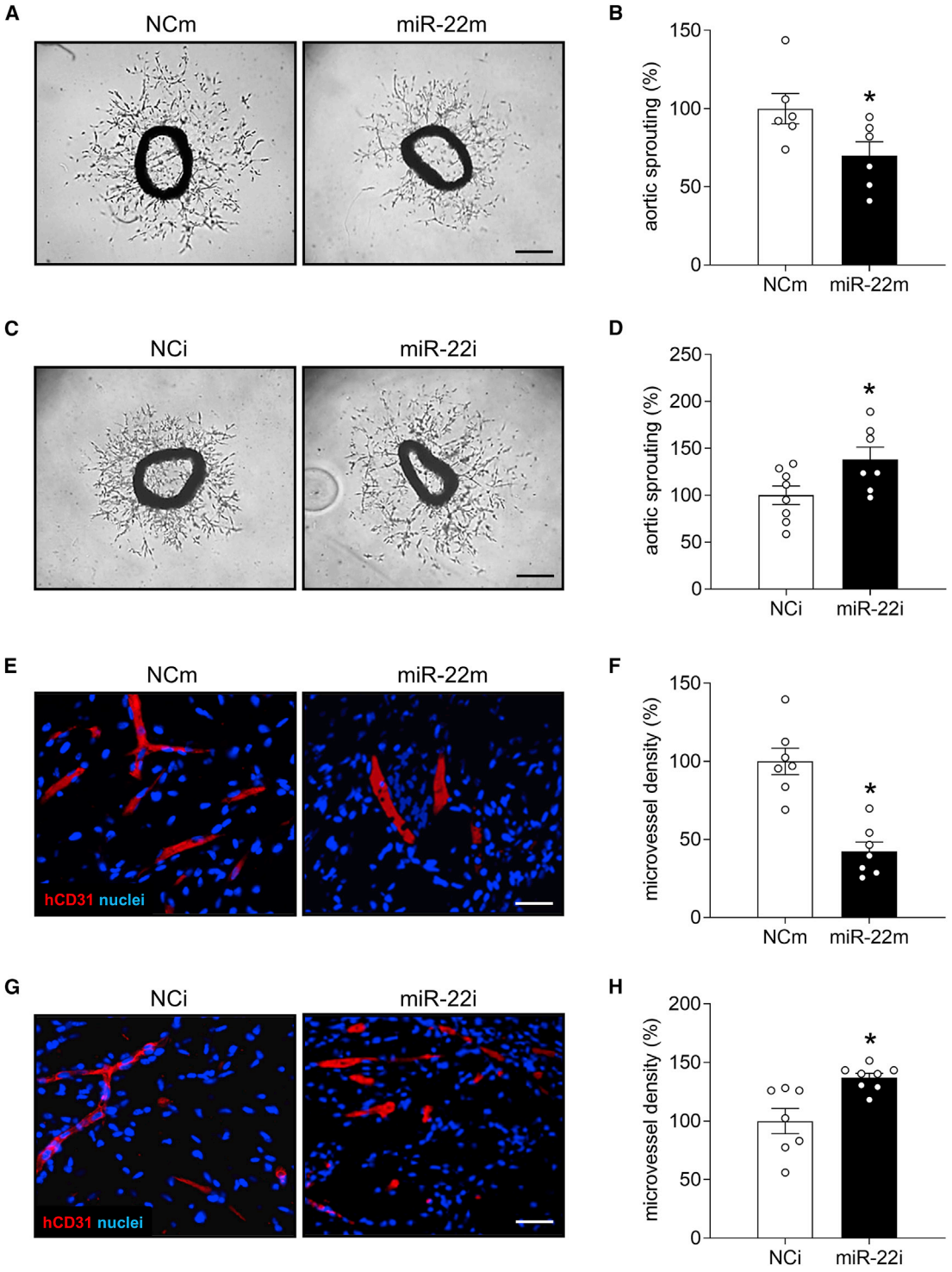

Figure 3. miR-22 suppresses angiogenesis *ex vivo* and *in vivo*

(A and C) Phase-contrast microscopic images of mouse aortic rings, which were transfected with miR-22m (A), miR-22i (C), or corresponding scrambled NCm (A) and NCi (C) overnight and then cultured in Matrigel for 6 days. Scale bars, 400 μm. (B and D) Sprouting (in % of NCm or NCi) of aortic rings that were transfected with miR-22m (B), miR-22i (D), or corresponding scrambled NCm (B) and NCi (D), as assessed by computer-assisted image analysis (n = 6 to 8). (E and G) Immunohistochemical detection of human

(legend continued on next page)

transfected controls (Figures 4A, 4C, and 4D). Accordingly, tumors containing miR-22m-transfected HDMECs also exhibited a markedly reduced final tumor weight (Figure 4B). As expected, overexpression of miR-22 in HDMECs significantly counteracted the tumor cell-stimulated development of human microvessels within the tumors, but not the angiogenic ingrowth of mouse microvessels from the surrounding host tissue (Figures 4E and 4F). Additional immunohistochemical analyses demonstrated that tumors containing miR-22m-transfected HDMECs exhibited less Ki67-positive but more cleaved caspase (casp)-3-positive tumor cells when compared to controls (Figures 4G–4J). This indicates that miR-22 overexpression in tumor ECs inhibits the proliferation of tumor cells and also promotes their apoptotic cell death.

miR-22 targets *SIRT1* and *FGFR1* in ECs

To identify the functional targets of miR-22 that mediate its antiangiogenic effects in ECs, we first analyzed the predicted human target genes of miR-22 according to the algorithms of miRDB and TargetScan. We detected five genes that are involved in angiogenesis and have not been validated as miR-22 targets, which encode tumor necrosis factor receptor (TNFR) 2, vascular endothelial zinc finger (VEZF) 1, transforming growth factor beta-activated kinase (TAK) 1, serine–arginine protein kinase (SRPK) 1, and protein kinase C beta (PRKCB). However, none of these genes were downregulated in miR-22m-transfected HDMECs when compared to NCm-transfected controls (Figure 5A). These findings indicate that these five genes may not be the functional targets of miR-22 and therefore were not evaluated further, since it is well known that miRNA regulates gene expression mainly through mRNA degradation.[9,19]

Next, we analyzed the validated human targets of this miRNA based on the current literature and found 13 angiogenesis-related genes. These genes encode brain-derived neurotrophic factor (BDNF), cysteine-rich protein (CYR) 61, cluster of differentiation (CD) 151, lysine-specific demethylase (KDM) 3A, specificity protein (SP) 1, neuroepithelial cell transforming (NET) 1, CD147, high mobility group box protein (HMGB) 1, DNA damage inducible transcript (DDIT) 4, neuroblastoma RAS viral oncogene homolog (NRAS), metadherin (MTDH), SIRT1, and FGFR1. By performing real-time PCR assays, the mRNA levels of *SIRT1* and *FGFR1* were found to be significantly decreased in miR-22m-transfected HDMECs when compared to NCm-transfected controls (Figure 5A). Consistently, the protein levels of *SIRT1* and *FGFR1* were markedly decreased by miR-22 overexpression, as assessed by western blot analysis (Figures 5B and 5C). Recently, Hu et al.[20] reported that miR-22 targets *FGFR1* in human liver Huh7 cells. We further confirmed this finding in 293T cells; 293T is a highly transfectable cell line and is widely used for miRNA target validation. For this purpose, a dual luciferase assay was performed by cotransfecting miR-22m and *FGFR1*-3′ UTR luciferase reporter plasmid (wild-type) or an empty plasmid with deletion of *FGFR1*-3′ UTR (mutant) into the cells. We found that miR-22m significantly attenuates the activity of the *FGFR1*-3′ UTR luciferase reporter, whereas no reduction was detected upon cotransfection with mutant plasmid (Figure 5D).

Given the fact that both SIRT1 and FGFR1 are upstream proteins of the pivotal angiogenesis regulatory pathway AKT/mTOR, we performed western blot analyses to assess the activation of this pathway in NCm- and miR-22m-transfected HDMECs. As expected, transfection with miR-22m markedly reduced the phosphorylation of AKT and mTOR by 52% and 48%, respectively (Figures 5E–5G).

miR-22 inhibits angiogenesis through targeting *SIRT1* and *FGFR1*

Previous studies suggest an important role of SIRT1 and FGFR1 in regulating angiogenesis.[5,21] To determine whether miR-22 inhibits the angiogenic activity of ECs through targeting *SIRT1* and *FGFR1*, the specific SIRT1 inhibitor EX-527 and the selective FGFR1 inhibitor PD173074 were used in an additional panel of *in vitro* assays. By means of a WST-1 assay, we found that 10–50 μM of EX-527 and 50–500 nM of PD173074 significantly reduce the viability of HDMECs after 3 days of treatment (Figures 6A and 6B). Accordingly, to avoid cytotoxic effects of these compounds, we chose a minimal effective dose of each inhibitor (i.e., 10 μM of EX-527 and 50 nM of PD173074) for the following WST-1, scratch wound healing, and tube formation assays. These functional analyses revealed that exposure to EX-527 and PD173074 completely reverses miR-22i-promoted HDMEC viability, migration, and tube formation (Figures 6C–6E).

Furthermore, we analyzed whether miR-22 functions through suppressing AKT/mTOR signaling, which is a common downstream pathway of SIRT1 and FGFR1, using the highly specific AKT inhibitor MK-2206. In a previous publication,[22] we found that 5–40 μM of MK-2206 significantly reduces HDMEC viability after 3 days of incubation. Accordingly, miR-22i-transfected HDMECs were exposed to 5 μM of MK-2206, followed by the WST-1, scratch wound healing, and tube formation assays. By this, we could demonstrate that inhibition of AKT completely counteracts miR-22i-enhanced HDMEC viability, migration, and tube formation (Figures 6F–6H).

Because we found that NSCLC cells downregulate endothelial miR-22 by activating NF-κB possibly via secreting IL-1β, we investigated the regulation of the miR-22 targeted genes in ECs. For this purpose, we assessed the expression of *SIRT1* and *FGFR1* in IL-1β- or Bay 11-7082-exposed HDMECs as well as HDMECs cocultured with NCI-H460 cells. Real-time PCR assays revealed that IL-1β significantly

CD31-positive microvessels (red) in Matrigel plugs containing HDMECs transfected with miR-22m (E), miR-22i (G), or corresponding scrambled NCm (E) and NCi (G). Sections were additionally stained with Hoechst 33342 to identify cell nuclei (blue). Scale bars, 40 μm. (F and H) Microvessel density (in % of NCm or NCi) of Matrigel plugs containing HDMECs transfected with miR-22m (F), miR-22i (H), or corresponding scrambled NCm (F) and NCi (H), as assessed by immunohistochemistry (n = 7 to 8). Data are means ± SEM. *$p < 0.05$ versus NCm or NCi.

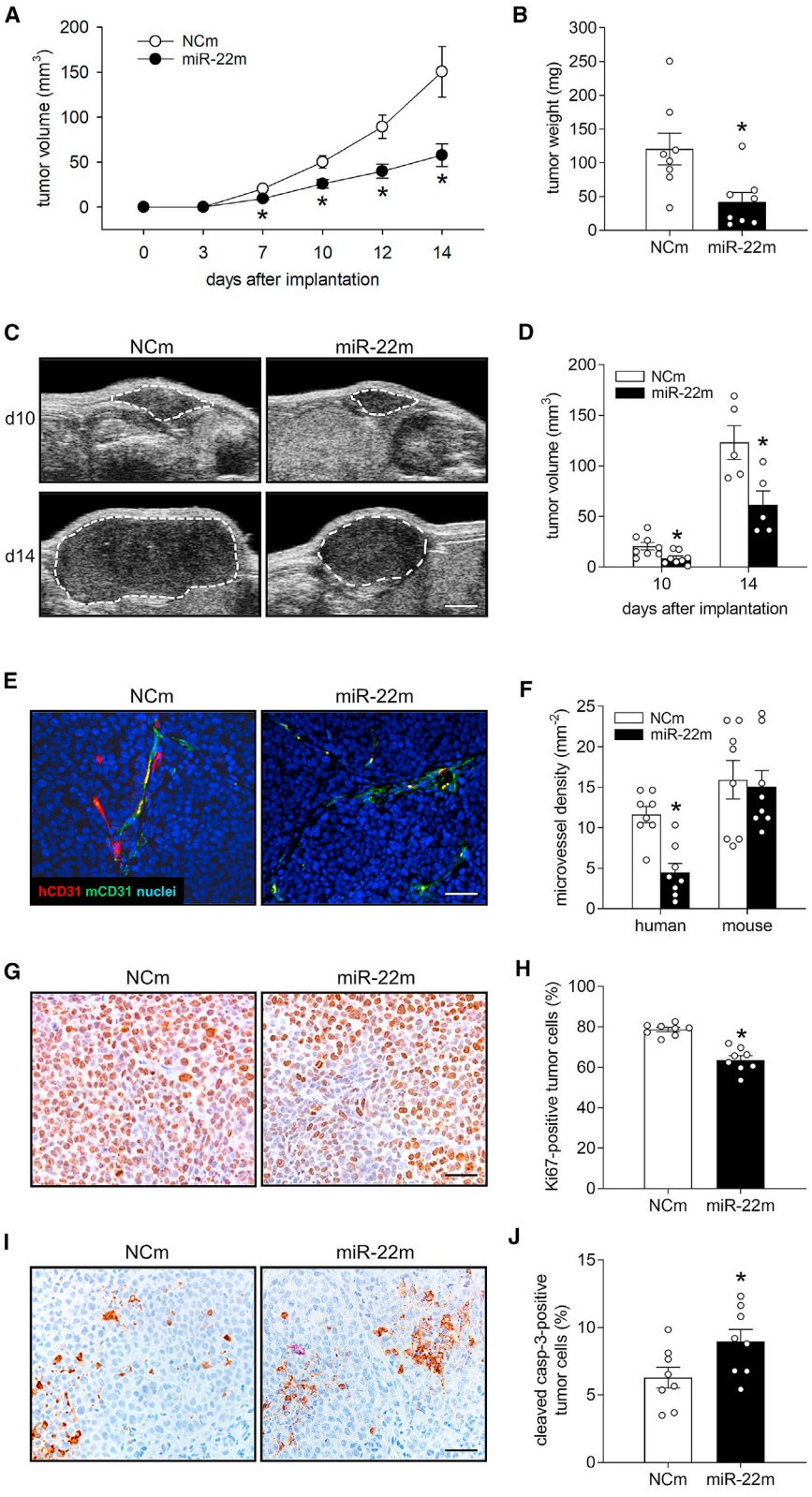

Figure 4. Endothelial miR-22 inhibits tumor angiogenesis and growth

(A) Volume (in mm^3) of developing NCI-H460 flank tumors containing NCm- or miR-22m-transfected HDMECs, as assessed by means of a digital caliper on the day of tumor induction (day 0) as well as on days 3, 7, 10, 12, and 14 (n = 8). (B) Final weight (in mg) of tumors containing NCm- or miR-22m-transfected HDMECs on day 14 (n = 8). (C) High-resolution ultrasound imaging of tumors containing NCm- or miR-22m-transfected HDMECs on days 10 and 14 after implantation. The borders of tumors are marked by white dashed lines. Scale bar, 1.8 mm. (D) Volume (in mm^3) of tumors containing NCm- or miR-22m-transfected HDMECs, as assessed by high-resolution ultrasound imaging on days 10 and 14 (n = 5 to 8). (E) Immunohistochemical detection of newly formed human (red) and mouse (green) microvessels in tumors containing NCm- or miR-22m-transfected HDMECs on day 14 (n = 8). Sections were stained with Hoechst 33342 to identify cell nuclei (blue). Scale bar, 60 μm. (F) Density (in mm^{-2}) of human and mouse microvessels in tumors containing NCm- or miR-22m-transfected HDMECs on day 14 (n = 8). (G and I) Immunohistochemical detection of human Ki67- (G) or cleaved casp-3-positive (I) tumor cells within NCI-H460 xenografts containing NCm- or miR-22m-transfected HDMECs. Scale bars: 25 μm. (H and J) Ki67-positive (H) or cleaved casp-3-positive cells (J) (in % of the total number of nuclei) within NCI-H460 xenografts containing NCm- or miR-22m-transfected HDMECs (n = 8). Data are means ± SEM. *$p < 0.05$ versus NCm.

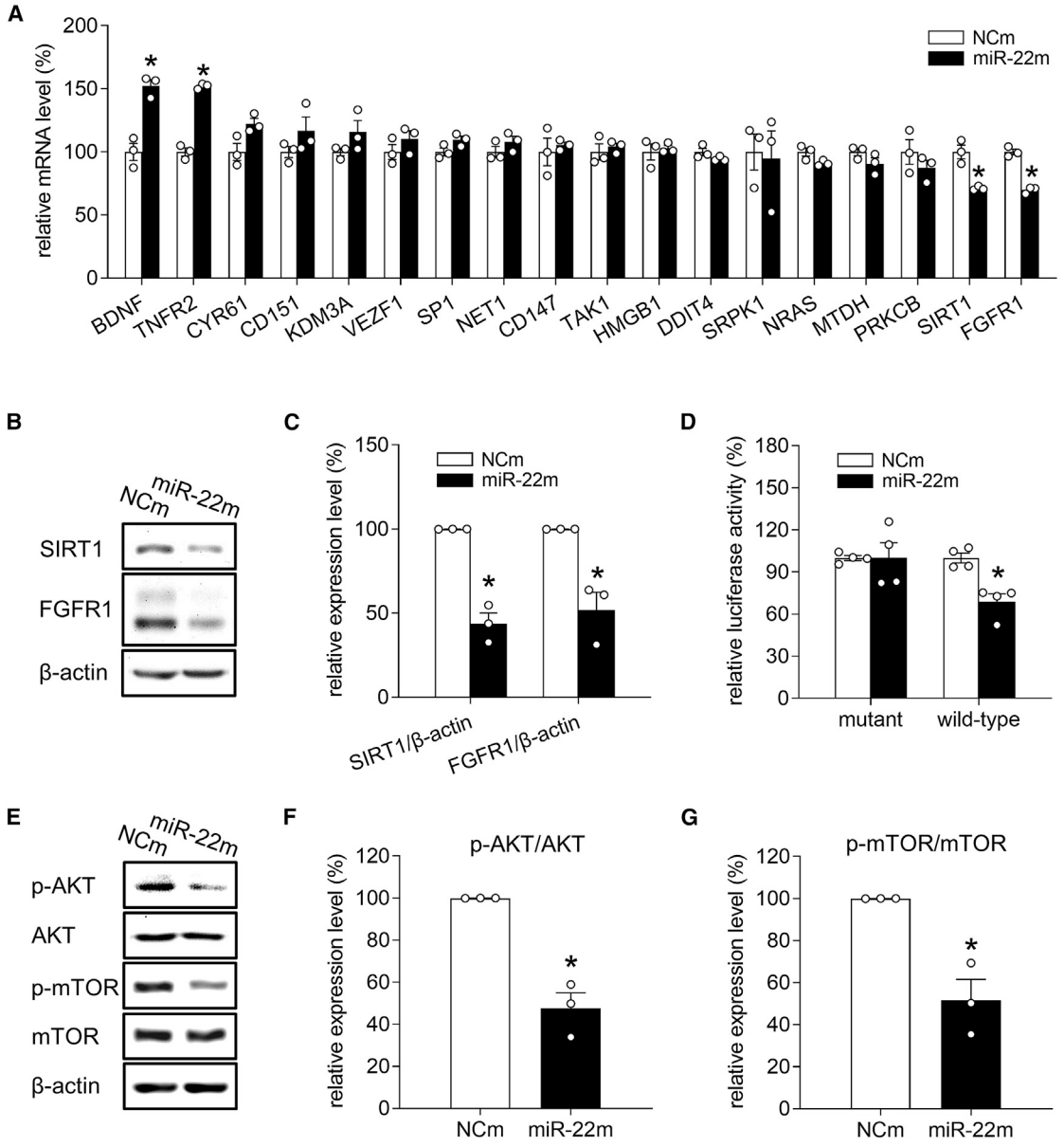

Figure 5. miR-22 targets *SIRT1* and *FGFR1* in ECs

(A) mRNA levels (in % of NCm) of putative and validated human target genes of miR-22 in NCm- or miR-22m-transfected HDMECs, as assessed by real-time PCR (n = 3). (B) Western blots of SIRT1, FGFR1, and β-actin expression in HDMECs transfected with NCm or miR-22m. (C) Expression level (in % of NCm) of SIRT1/β-actin and FGFR1/β-actin, as assessed by western blotting (n = 3). (D) Luciferase activity (in % of NCm) in 293T cells cotransfected with NCm or miR-22m and a reporter plasmid carrying mutant or wild-type *FGFR1-3′* UTR, as assessed by the luciferase assay (n = 4). (E) Western blots of p-AKT, AKT, p-mTOR, mTOR, and β-actin expression in HDMECs transfected with NCm or miR-22m. (F and G) Expression levels (in % of NCm) of p-AKT/AKT (F) and p-mTOR/mTOR (G), as assessed by western blotting (n = 3). Data are means ± SEM. *$p < 0.05$ versus NCm.

promotes the expression of *SIRT1* but not that of *FGFR1* (Figures 6I and 6J). In contrast, Bay 11-7082 reduced the expression of both genes (Figures 6I and 6J). Moreover, noncontact coculture of HDMECs with NCI-H460 cells significantly upregulated the endothelial expression of *SIRT1* and *FGFR1*, whereas inhibition of NF-κB with Bay 11-7082 reversed this upregulation (Figures 6K and 6L).

DISCUSSION

miR-22 has been widely studied in tumorigenesis, where it acts as a tumor suppressor or an oncogene by regulating the proliferation, migration, invasion, metastasis, apoptosis, senescence, and epithelial-mesenchymal transition of different types of tumor cells.[11] In contrast, our study focused on the effects of miR-22 on the angiogenic

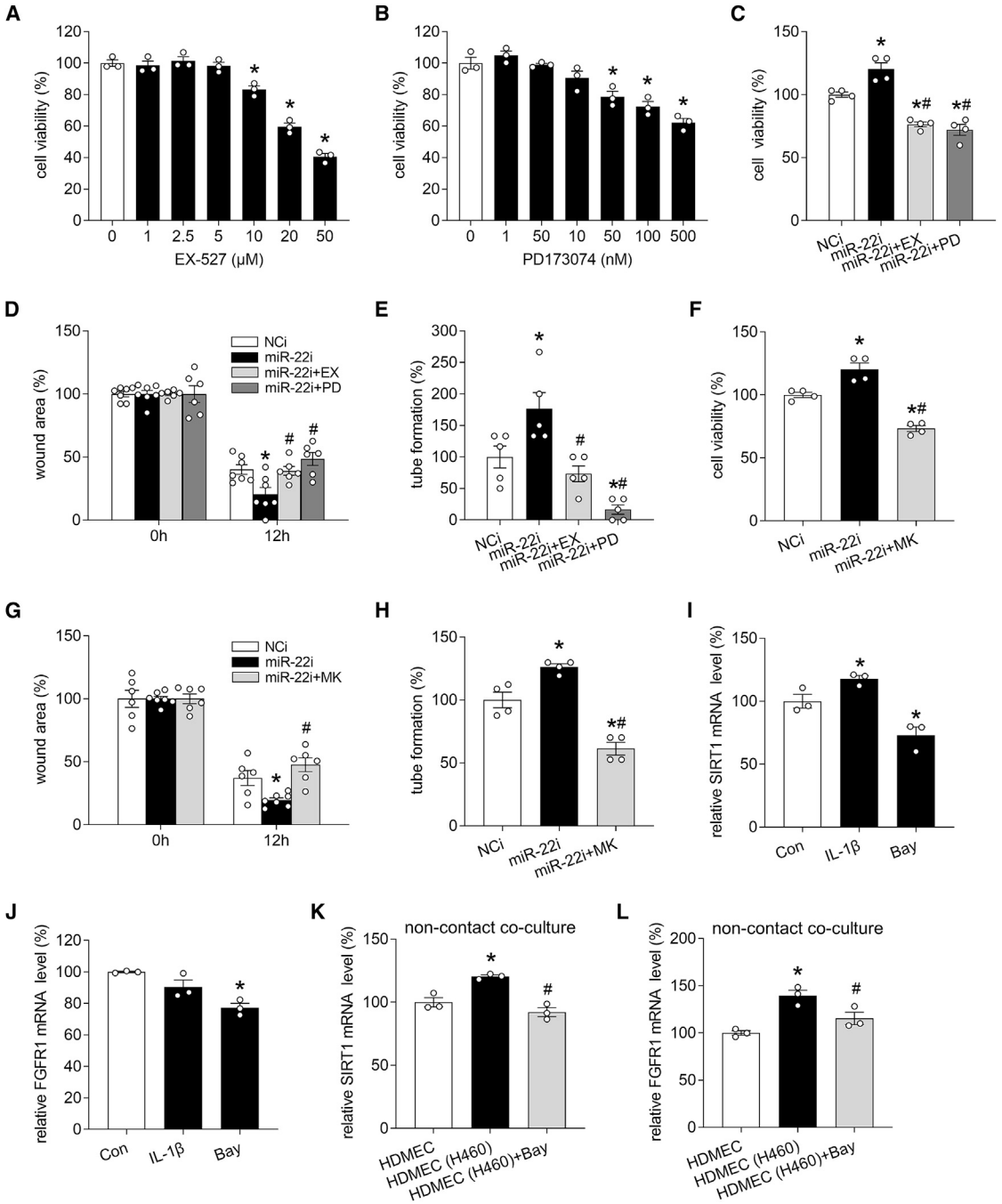

Figure 6. miR-22 inhibits angiogenesis through targeting *SIRT1* and *FGFR1*

(A and B) Viability (in % of 0 μM or 0 nM) of HDMECs that were exposed for 72 h to serial dilutions of EX-527 (A) and PD173074 (B), as assessed by the WST-1 assay (n = 3). (C) Viability (in % of NCi) of HDMECs that were transfected with NCi or miR-22i and then treated with 10 μM of EX-527 (EX) or 50 nM of PD173074 (PD) for 72 h, as assessed by the WST-1 assay (n = 4). (D) Wound area (in % of 0 h) created by scratching the monolayer of HDMECs that were transfected with NCi or miR-22i and then treated with 10 μM of EX-527 or 50 nM of PD173074 for 12 h, as assessed by the scratch wound healing assay (n = 6 to 7). (E) Tube formation (in % of NCi) of HDMECs that were transfected with NCi or miR-22i and then treated with 10 μM of EX-527 or 50 nM of PD173074 for 18 h, as assessed by the tube formation assay (n = 5). (F) Viability (in % of NCi) of HDMECs that were transfected with NCi or miR-22i and then treated with 5 μM of MK-2206 (MK) for 72 h, as assessed by the WST-1 assay (n = 4). (G) Wound area (in % of 0 h) created by scratching the monolayer of HDMECs that were transfected with NCi or miR-22i and then treated with 5 μM of MK-2206 for 12 h, as assessed by the scratch wound healing assay (n = 6). (H) Tube formation (in % of NCi) of HDMECs that were transfected with NCi or miR-22i and then treated with 5 μM of MK-2206 for 18 h, as assessed by

(legend continued on next page)

activity of ECs. Although miR-22 was found to induce endothelial progenitor cell senescence and its injection into zebrafish embryos causes defective vascular development,[23,24] the regulation, function, and targets of miR-22 in ECs still remain elusive. Our findings demonstrate that miR-22 is preferentially and highly expressed in ECs and the suppression of endothelial miR-22 mediates NSCLC cell-stimulated blood vessel formation. In fact, NSCLC cells activate endothelial NF-κB possibly via releasing IL-1β and thus markedly reduce the high expression of miR-22 in ECs. This increases the angiogenic activity of ECs, because miR-22 functions as a potent angiogenesis inhibitor by targeting *SIRT1* and *FGFR1*.

Lung cancer is the most frequently diagnosed cancer and the leading cause of cancer death in both sexes worldwide.[25] NSCLC, including adenocarcinoma, large cell carcinoma, and squamous cell carcinoma, accounts for approximately 85% of all lung cancer cases. Despite recent advances in diagnosis and treatment, many patients with NSCLC still have limited treatment options and a poor prognosis.[26] Therefore, in the present study we focused on this specific tumor type and found miR-22 to be significantly downregulated in ECs microdissected from human NSCLC tissues when compared to that from matched nontumor lung tissues. *In vitro*, we also detected a significantly downregulated expression of miR-22 in HDMECs directly cocultured with NCI-H460 or NCI-H23 cells when compared to EC monocultures. This is in line with a previous study reporting that miR-22 expression in primary human brain microvascular ECs is reduced by contact coculture with U87 glioma cells.[27] Hence, endothelial miR-22 seems to be regulated by different types of tumors.

Tumor cells can directly interact with ECs via adhesion receptors and gap junctions. In addition, they can activate ECs by secreting soluble factors and microvesicles into the extracellular space as well as by changing the pH, oxygen, and nutrient levels in the surrounding microenvironment.[28] Our study revealed that NSCLC cells reduce endothelial miR-22 expression at least partially through secreting IL-1β. The proinflammatory cytokine IL-1β is widely accepted as a proangiogenic factor.[29] It exerts its biological functions through binding to the IL-1 receptor. This, in turn, recruits and activates the inhibitor of NF-κB (IκB) kinase complex. The consequent phosphorylation of IκB proteins leads to the translocation of NF-κB into the nucleus, where it promotes or represses the transcription of mRNAs and miRNAs.[17,18] Of interest, a recent study identified two NF-κB binding motifs in the miR-22 promoter that mediate the transcriptional repression of miR-22 in 182^{R}-6 breast cancer cells.[30] Our results now demonstrate that the exposure of HDMECs to the NF-κB inhibitor Bay 11-7082 significantly increases miR-22 expression, indicating that miR-22 is transcriptionally repressed by NF-κB not only in tumor cells but also in ECs.

We next investigated the effects of endothelial miR-22 on angiogenesis and tumor growth. By a panel of well-established *in vitro* angiogenesis assays, we could demonstrate that miR-22 is a pleiotropic angiogenesis inhibitor that targets all of the major steps of the angiogenic process, including EC proliferation, migration, and tube formation. Of note, the inhibitory effects of miR-22 on these steps were not directly dependent on each other. This is indicated by the observation that miR-22m inhibits HDMEC migration and tube formation within 24 h after transfection without affecting the viability of the cells. Our *in vitro* results were further confirmed by an *ex vivo* mouse aortic ring assay and an *in vivo* Matrigel plug assay. The fact that the mouse aortic ring assay is based on the angiogenic sprouting activity of murine ECs shows that the antiangiogenic effect of miR-22 is reproducible in ECs of different origin. To further evaluate the effects of endothelial miR-22 on NSCLC growth, we established an *in vivo* tumor cell-EC communication model by injecting NCm- or miR-22-transfected HDMECs admixed with NCI-H460 cells into the flanks of immunodeficient mice. It is important to mention that this modified flank tumor model only allows the manipulation of miR-22 expression in exogenous human ECs but not endogenous mouse ECs. However, these mouse ECs invade the developing tumor, assemble into new microvessels, and thus also support tumor growth. Accordingly, our model may underestimate the inhibitory effect of miR-22 on NSCLC growth.

Previous studies indicated that the interaction of miRNAs with their targets differs in diverse cell types and conditions due to the high complexity of cellular physiology.[31,32] Therefore, it was necessary in the present study to identify the specific functional targets of miR-22 in ECs. For this purpose, we analyzed both the putative and validated human target genes of miR-22. Among the 13 analyzed validated targets, only *SIRT1* and *FGFR1* were found to be downregulated in miR-22-overexpressing HDMECs, strongly supporting the view that miR-22 regulates its targets in a cell-type-dependent manner. FGFR1 is a member of the FGFR family of receptor tyrosine kinases and most commonly expressed on ECs.[21] Activation of FGFR1 by heparin-binding FGFs, mainly FGF1 and bFGF, increases the angiogenic activity of ECs *in vitro* and *in vivo*.[21] Thus, FGFR1 has been increasingly considered to be an attractive target for the antiangiogenic treatment of tumors. In order to investigate whether the suppression of *SIRT1* or *FGFR1* mediates the antiangiogenic function of miR-22, we exposed miR-22i-transfected HDMECs to the SIRT1 inhibitor EX-527 or the FGFR1 inhibitor PD173074. These small molecular inhibitors were used instead of short interfering RNAs (siRNAs) against *SIRT1* or *FGFR1*, because we found in preliminary experiments that the cotransfection efficiency of miR-22i and siRNAs is quite low in HDMECs.

There are several limitations of this study. One major limitation is the small size of patient samples. In fact, the number of included NSCLC

the tube formation assay (n = 4). (I and J) mRNA level of *SIRT1* (I) or *FGFR1* (J) (in % of Con) in HDMECs that were exposed for 72 h to vehicle (Con), 2 ng/mL of IL-1β, or 1 μM of Bay 11-7082 (Bay), as assessed by real-time PCR (n = 3). (K and L) mRNA level of *SIRT1* (K) or *FGFR1* (L) (in % of HDMEC) in HDMECs that were cultured alone (HDMEC) or cocultured with NCI-H460 cells [HDMEC (H460)] without contact in a transwell plate in the absence or presence of 1 μM of Bay 11-7082 (Bay) for 72 h, as assessed by real-time PCR (n = 3). Data are means ± SEM. *$p < 0.05$ versus 0 μM, 0 nM, NCi, Con, or HDMEC; $^{\#}p < 0.05$ versus miR-22i (C–H) or HDMEC (H460) (K and L).

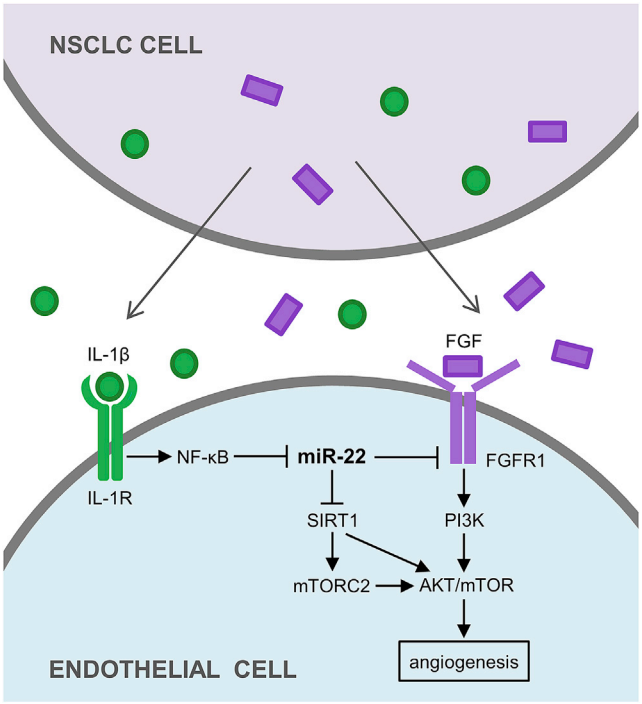

Figure 7. NSCLC cells stimulate angiogenesis by downregulating endothelial miR-22, which targets *SIRT1* and *FGFR1*

The scheme summarizes the underlying mechanisms, as outlined in detail in the Discussion.

patients was too small to determine the correlation between endothelial miR-22 and the patients' clinical characteristics with sufficient statistical power. However, this was not the major scope of the present study. This study was further limited by the lack of an efficient method for targeted delivery of miRNA into ECs *in vivo*.[33] This largely prevents our present approach to be directly translated into clinical practice. For this purpose, it will be necessary to develop miRNA modifications and sophisticated delivery systems to improve the safety, efficiency, and specificity of miRNA-based therapeutics. Rapid progress in chemical and bioengineering of miRNA, nanotechnology, and viral vector development may markedly contribute to achieve these goals in the future.

In conclusion, this study demonstrates that downregulation of endothelial miR-22 significantly contributes to NSCLC cell-stimulated angiogenesis. As summarized in Figure 7, NSCLC cell-released IL-1β binds to its receptors located on ECs, causing the intracellular activation of NF-κB. This, in turn, suppresses endothelial miR-22 expression. miR-22 targets the two pivotal proangiogenic regulators *SIRT1* and *FGFR1*, which results in the blockage of AKT/mTOR signaling and inhibition of angiogenesis. Thus, the NF-κB-induced suppression of miR-22 results in an increased SIRT1- and FGFR1-mediated angiogenesis. Taken together, this mechanism indicates that endothelial miR-22 may represent a promising therapeutic target for the treatment of NSCLC.

MATERIALS AND METHODS

Study design

The main objective of our study was to analyze the function of endothelial miR-22 in regulating NSCLC angiogenesis. After identification of endothelial miR-22 to be significantly downregulated in human NSCLC tissue from 12 patients, the following studies were designed. First, contact and noncontact coculture systems were established *in vitro* using human ECs and NSCLC cells to study the regulation of endothelial miR-22 by NSCLC cells. Second, a panel of *in vitro* assays were exploited to investigate the effects of miR-22 on major angiogenic steps, including EC proliferation, migration, and tube formation. A mimic and an inhibitor of miR-22 were transfected into ECs to perform gain- and loss-of-function studies. Third, a Matrigel plug assay and a mouse flank tumor model were performed to confirm the *in vivo* inhibitory effects of miR-22 on angiogenesis and tumor growth. Fourth, real-time PCR, western blotting, and luciferase assays were used to identify and verify the target genes of miR-22. In this study, the sample size was estimated based on previous publications and experience. For each *in vitro* assay, at least three independent experiments with at least three biological replicates were performed to ensure the reproducibility and replicability of the results. Biological replicates are defined as separate cell cultures processed at the same time. Each mouse model included at least five mice in each group. These *in vivo* experiments could not be randomized, but all of the analyses were performed by the investigators blinded to group assignment. All collected data were included in the analysis and no outliers were excluded.

Chemicals

The NF-κB inhibitor Bay 11-7082, SIRT1 inhibitor EX-527, and FGFR1 inhibitor PD173074 were purchased from Santa Cruz Biotechnology (Heidelberg, Germany). The AKT inhibitor MK-2206 2HCL (MK-2206) was purchased from SelleckChem (Munich, Germany).

Patient samples

Human NSCLC tissues and matched adjacent nontumor lung tissues were obtained from 12 patients with lung adenocarcinoma. The pathological characteristics of these patients are shown in Table S1. All samples were dissected by professional pathologists at Saarland University Hospital, fixed in 4% formalin, and embedded in paraffin. This study was approved by the local ethics committee (permit number 01/08) and the patients provided informed consent.

LCM

Sections of lung adenocarcinoma and matched adjacent nontumor lung tissue, with a thickness of 5 μm, were mounted on MembraneSlides (Leica Microsystems, Wetzlar, Germany) and stained with hematoxylin and eosin. By using a microdissection microscope (Leica AS LMD), ECs were dissected and catapulted into the cap of 0.5-mL tubes (Leica Microsystems) after the removal of blood cells from capillaries. Approximately 2,000 ECs were retrieved from each sample. This procedure was assisted by an experienced pathologist.

Cell culture

HDMECs (PromoCell, Heidelberg, Germany) were cultured in endothelial cell growth medium (EGM)-MV (PromoCell). HUVECs (PromoCell) were cultured in EGM (PromoCell). NHDFs (a kind gift from Dr. Wolfgang Metzger, Department of Trauma, Hand and Reconstructive Surgery, Saarland University, Germany) and 293T human embryonic kidney cells (ATCC, Wesel, Germany) were cultured in Dulbecco's modified Eagle's medium (DMEM; PAA, Cölbe, Germany) supplemented with 10% fetal calf serum (FCS), 100 U/mL of penicillin, and 0.1 mg/mL of streptomycin (PAA). hPC-PLs (PromoCell) were cultured in pericyte growth medium (PromoCell). The human NSCLC cell lines NCI-H460 and NCI-H23 (ATCC) were maintained in RPMI 1640 medium supplemented with 10% FCS, 100 U/mL of penicillin, and 0.1 mg/mL of streptomycin. All cells were incubated at 37°C in a humidified atmosphere containing 5% CO_2.

Cell coculture

Contact and noncontact coculture systems were used to assess the influence of tumor cells on endothelial miR-22 expression. For contact coculture, 1×10^6 HDMECs with or without 5×10^6 NCI-H460 or NCI-H23 cells were seeded into 100-mm dishes and cultured in FCS-free endothelial cell basal medium (EBM; PromoCell) for 24 h. HDMECs were then isolated using a human CD31 MicroBead kit (Miltenyi Biotec, Bergisch Gladbach, Germany) according to the manufacturer's instructions. Briefly, the cocultured cells were detached with accutase (PAA) and suspended in 100 μL of EBM. Subsequently, 30 μL of FcR blocking reagent and 30 μL of CD31 MicroBeads were added, followed by incubation at 4°C for 15 min. After 1 mL of EBM was added, the cells were sequentially collected by centrifugation, resuspended in 1 mL of EBM, and applied onto the LS columns in the magnetic field of a MidiMACS separator. The column was washed 10 times with 3 mL of EBM and then removed from the separator. The retained ECs were flushed out three times with 4 mL of EBM by pushing the plunger into the column and collected for further purity assessment and RNA extraction. For noncontact coculture, six-well transwell plates containing inserts with 0.4-μm pores (Corning, Wiesbaden, Germany) were used, which allowed soluble factors but not cells to pass through. A number of 1×10^5 NSCLC cells were loaded onto the inserts and 2×10^5 HDMECs were plated in the wells. After culture for 24 h in EBM in the absence or presence of Bay 11-7082, immunoglobulin G (IgG; R&D Systems, Wiesbaden, Germany), anti-TNF-α NAb (R&D Systems), or anti-IL-1β NAb (R&D Systems), HDMECs were collected for RNA extraction.

Immunocytochemistry

To check the cellular localization of p65, HDMECs were seeded on coverslips placed in a six-well transwell plate and NCI-H460 cells were loaded onto the inserts. After culture in EBM for 4 h, HDMECs were fixed in 3.7% paraformaldehyde for 30 min, permeabilized with 0.5% Triton X-100 for 10 min, and blocked with 2% bovine serum albumin for 15 min. Afterward, the cells were incubated with a primary antibody against p65 (1:25; R&D Systems) for 1 h, followed by the incubation with a Cy3-conjugated secondary antibody (1:250; Abcam, Cambridge, UK) for another 1 h. Cell nuclei were stained with Hoechst 33342 (Sigma-Aldrich, Taufkirchen, Germany). The percentage of p65-positive nuclei was quantified in eight regions of interest (ROIs) of each coverslip at 400× magnification with a BX-60 microscope (Olympus, Hamburg, Germany).

Cell transfection

To investigate the function of miR-22 in HDMECs, the cells were transfected with miR-22m (QIAGEN, Hilden, Germany) or miR-22i (QIAGEN) for 48 h to up- or downregulate intracellular miR-22, respectively. HiPerFect transfection reagent (QIAGEN) was used according to the manufacturer's protocol. Cells transfected with NCm (QIAGEN) or NCi (QIAGEN) served as controls.

WST-1 assay

To assess cell viability, WST-1 assays (Roche Diagnostics, Mannheim, Germany) were performed according to the manufacturer's instructions. Briefly, 4×10^3 HDMECs were seeded in 96-well plates and incubated for the indicated time periods. Then, 10 μL of WST-1 reagent was added into each well. After 30 min of incubation, the absorbance of each well was measured at 450 nm by a microplate reader (PHOmo; Anthos Mikrosysteme GmbH, Krefeld, Germany), with 620 nm as the reference. The control group was assigned a value of 100%.

Flow cytometry

To analyze the purity of isolated HDMECs, the cells were incubated with a fluorescein isothiocyanate-conjugated mouse anti-human CD31 antibody (1:50; BD PharMingen, San Diego, CA) for 30 min at room temperature followed by three washes with phosphate-buffered saline (PBS). At least 10,000 events were acquired using a FACScan flow cytometer (BD Biosciences, Heidelberg, Germany) and analyzed with CellQuest Pro software (BD Biosciences).

The function of miR-22 in cell cycle regulation was also detected by flow cytometry as previously described.[34] Briefly, transfected HDMECs were reseeded and incubated for 24 h. The cells were then collected and fixed, followed by staining with propidium iodide and digestion with RNase A (Sigma-Aldrich). Subsequently, the cell cycle distribution was assessed with the FACScan flow cytometer and the DNA histograms of 10,000 cells were analyzed with BD CellQuest Pro software.

Cell migration assay

To evaluate EC motility, two different migration assays were performed. For the scratch wound healing assay, HDMECs were seeded in 35-mm culture dishes. After reaching confluence, the cell monolayer was scratched with a 10-μL pipette tip to generate scratch wounds and then rinsed with PBS to remove nonadherent cells. Phase-contrast microscopy (BZ-8000; Keyence, Osaka, Japan) was used to observe the wounds immediately after scratching (0 h) as well as after 12 or 24 h. The wound area was measured and expressed as a percentage of corresponding NCm or NCi controls.

The transwell migration assay was performed as previously described.[35] Briefly, 2.5×10^5 transfected HDMECs in 500 µL of EBM were seeded into an insert of 24-transwell plates with 8-µm pores (Corning) and 750 µL of EBM supplemented with 1% FCS was added to the lower well. Cells were allowed to migrate for 5 h and thereafter stained with Dade Diff-Quick (Dade Diagnostika GmbH, Munich, Germany). Cell migration was quantified by counting the number of migrated cells in 20 ROIs at 200× magnification using a BZ-8000 microscope (Keyence) and expressed as a percentage of corresponding NCm or NCi controls.

Tube formation assay

To assess the tube-forming activity of ECs, 1.5×10^4 transfected HDMECs were added into each well of a 96-well plate precoated with 50 µL of Matrigel (∼10 mg/mL; Corning). After incubation for 18 h, the formation of tubular structures was observed under phase-contrast microscopy (BZ-8000; Keyence). Tube formation was quantified by analyzing the number of meshes (i.e., areas completely surrounded by endothelial tubes) with ImageJ software (US National Institutes of Health, Bethesda, MD) and expressed as a percentage of corresponding NCm or NCi controls.

Aortic ring assay

To investigate the function of miR-22 in aortic sprouting, aortic rings processed from male BALB/c mice (8 weeks old) were transfected for 18 h with 50 nM of miR-22m, 1 µM of miR-22i, or scrambled NCm and NCi and then embedded in Matrigel (∼10 mg/mL; Corning) in a 96-well plate. After Matrigel polymerization, DMEM supplemented with 10% FCS was added into each well and sprouts from the aortic wall were allowed to develop for 6 days, followed by observation with phase-contrast microscopy (BZ-8000; Keyence). Aortic sprouting was quantified by measuring the area of the outer aortic vessel sprouting and expressed as a percentage of corresponding NCm or NCi controls.

Animal models

All animal experiments were approved by the local governmental animal protection committee (permit number 22/2014) and were conducted according to the German legislation for animal welfare and the Guide for the Care and Use of Laboratory Animals (8th edition, 2011).

To investigate the *in vivo* function of miR-22 in angiogenesis, a Matrigel plug assay was performed as previously described.[22] Briefly, transfected HDMECs in EBM (1×10^7 cells/mL) were mixed with the same volume of growth factor-reduced Matrigel (∼20 mg/mL; Corning) and then supplemented with 1 µg/mL of VEGF (R&D Systems), 1 µg/mL of bFGF (R&D Systems), and 50 IU/mL of heparin (B. Braun, Melsungen, Germany). Then, 300 µL of Matrigel admixed with HDMECs was subcutaneously injected into 8- to 10-week-old CD1 nude mice (∼25 g). The Matrigel plugs were collected for immunohistochemical analyses 7 days after implantation.

The function of endothelial miR-22 in tumor angiogenesis and growth was evaluated in a flank tumor model. For this purpose, 1.5×10^5 NCI-H460 cells in combination with 1.5×10^6 NCm- or miR-22m-transfected HDMECs were suspended in 50 µL of EGM-MV and injected subcutaneously into the flanks of 8-week-old NOD-SCID (NOD. CB17/AIhnRj-Prkdc^{scid}) mice (Janvier Labs, Le Genest-St-Isle, France). Two perpendicular diameters of the developing tumors were repetitively measured on days 0, 3, 7, 10, and 14 by means of a caliper. The tumor volumes were calculated using the formula $V = 1/2\ (L \times W^2)$, where L was the longer diameter and W was the shorter diameter.[36] The tumor development was also assessed using a combined ultrasound and photoacoustic imaging system (Vevo LAZR) with a LZ550 scanhead (40-MHz center frequency) (FUJIFILM VisualSonics Inc, Toronto, ON, Canada) on days 10 and 14 after implantation. The ultrasound images of tumors were analyzed by means of a three-dimensional reconstruction using VisualSonics software (Vevo LAB 1.7.2.). At the end of the experiment (i.e., on day 14), the tumors were carefully excised, weighed, and further processed for immunohistochemical analyses.

Immunohistochemistry

Formalin-fixed specimens of Matrigel plugs and tumors were embedded in paraffin and 2-µm sections were cut. To detect the neovascularization of the plugs and tumors, the sections were stained with a rabbit anti-human CD31 antibody (1:100; Abcam) or a rabbit anti-mouse CD31 antibody (1:100; Abcam), followed by a goat anti-rabbit Alexa Fluor 555-labeled secondary antibody (1:100; Life Technologies; Thermo Fisher Scientific, Karlsruhe, Germany) or a goat anti-rat Alexa Fluor 488-labeled secondary antibody (1:100; Life Technologies). Cell nuclei were stained with Hoechst 33342 (Sigma-Aldrich). The sections were subsequently examined using a fluorescence microscope (BX60; Olympus). Microvessel density was quantified by counting the numbers of CD31-positive microvessels in 10 ROIs of each section at 200× magnification. To evaluate the proliferation and apoptosis of tumor cells, sections were stained with a monoclonal rabbit antibody against Ki67 (1:400; Cell Signaling Technology, Frankfurt, Germany) or a polyclonal rabbit antibody against cleaved casp-3 (1:100; New England Biolabs, Frankfurt, Germany), followed by a biotinylated goat anti-rabbit secondary antibody (Abcam) and streptavidin-peroxidase conjugate (ready-to-use; Abcam). The staining was completed by incubation with 3-amino-9-ethylcarbazole substrate (Abcam) before the sections were counterstained with Mayer's hemalum solution (HX948000; Merck, Darmstadt, Germany). The percentages of Ki67-positive proliferating and cleaved casp-3-positive apoptotic tumor cells were quantified in 12 ROIs on each section at 400× magnification with a BX-60 microscope (Olympus).

Quantitative real-time PCR

Total RNA was extracted using a RNeasy FFPE Kit (QIAGEN), RNeasy Mini kit (QIAGEN), or miRNeasy Mini kit (QIAGEN) following the manufacturer's instructions. Then the extracted RNA was processed for the reverse transcription reaction by utilizing a QuantiTect Reverse Transcription Kit (QIAGEN) or miScript II RT

Kit (QIAGEN). It is noteworthy that after reverse transcription, cDNA of dissected ECs by LCM was further amplified using the RT^2 PreAMP cDNA Synthesis Kit (QIAGEN) or the miScript PreAMP PCR Kit (QIAGEN). Quantitative real-time PCR was performed and analyzed in a MiniOpticon Real-Time PCR System (Bio-Rad, Munich, Germany) using the QuantiTect SYBR green PCR Kit (QIAGEN) or miScript SYBR Green PCR Kit. The relative expression levels of genes and miRNAs were calculated using the $2^{-\Delta\Delta Ct}$ method with glyceraldehyde 3-phosphate dehydrogenase (GAPDH) and U6 small nuclear RNA as endogenous controls, respectively. Gene-specific primer sequences are listed in Table S3. To analyze mature miRNA expression, miScript primer assays for Hs_miR-22_1 and Hs_RNU6-2_11 from QIAGEN were used.

Western blot analysis

As previously described,[37] whole cell lysates were separated on 8% sodium dodecyl sulfate polyacrylamide gels and transferred to polyvinylidene difluoride membranes (Bio-Rad). The membranes were blocked and incubated overnight at 4°C with a mouse monoclonal anti-FGFR1 antibody (1:100; Cell Signaling Technology), a rabbit polyclonal anti-p-AKT antibody (1:500; Cell Signaling Technology), a rabbit monoclonal anti-AKT antibody (1:500; Cell Signaling Technology), a rabbit monoclonal anti-p-mTOR (1:500; Cell Signaling Technology), a rabbit monoclonal anti-mTOR (1:500; Cell Signaling Technology), or a mouse monoclonal anti-β-actin antibody (1:2,000; Sigma-Aldrich). This was followed by the corresponding horseradish peroxidase-conjugated secondary antibodies (1:3,000; GE Healthcare, Freiburg, Germany). An electrochemiluminescence assay (GE Healthcare) was then performed and signals were acquired using a ChemoCam Imager (Intas, Göttingen, Germany). The intensities of protein bands were analyzed using ImageJ software (US National Institutes of Health).

Luciferase assay

For target validation, a control luciferase reporter plasmid (CmiT000001-MT06; GeneCopoeia, Rockville, MD) or *FGFR1*-3′ UTR target plasmid (HmiT005432-MT06; GeneCopoeia) was co-transfected with 50 nM of NCm or miR-22m into 293T cells using Lipofectamine 2000 (Invitrogen; Thermo Fischer Scientific). After 48 h of incubation, Renilla and Firefly luciferase activities were measured with the Dual-Luciferase Reporter Assay Kit 2.0 (GeneCopoeia) using a Tecan Infinite 200 Pro microplate reader (Tecan, Crailsheim, Germany). Relative luciferase activity was quantified by normalizing the Firefly luciferase signal to that of Renilla luciferase and expressed as a percentage of NCm controls.

Statistical analysis

Statistical comparisons between two groups were made with the paired Student's t test (for the analysis of patient samples) or the unpaired Student's t test using GraphPad Prism 9 software. Statistical comparisons between multiple groups were made by one-way ANOVA followed by the Tukey's multiple comparisons test using GraphPad Prism 9. All data are expressed as means ± SEM. A value of $p < 0.05$ was considered significant.

SUPPLEMENTAL INFORMATION

Supplemental information can be found online at https://doi.org/10.1016/j.omtn.2021.10.003.

ACKNOWLEDGMENTS

We are grateful for the excellent technical assistance of Janine Becker, Christina Max, and Ruth Nickels (all from the Institute for Clinical and Experimental Surgery, Saarland University). This work was supported by a research grant to Y.G. from the Medical Faculty of Saarland University (HOMFORexzellent 2015).

AUTHOR CONTRIBUTIONS

Y.G., E.M., R.M.B., Y.Z., and M.W.L. designed the research; Y.G., G.P., V.B., C.K., E.A., E.E., J.H., and N.L. performed the research; Y.G., G.P., V.B., C.K., E.A., and N.L. analyzed the data; Y.G., M.W.L., and M.D.M. wrote the paper.

DECLARATION OF INTERESTS

The authors declare no competing interests.

REFERENCES

1. Fontanini, G., Lucchi, M., Vignati, S., Mussi, A., Ciardiello, F., De Laurentiis, M., De Placido, S., Basolo, F., Angeletti, C.A., and Bevilacqua, G. (1997). Angiogenesis as a prognostic indicator of survival in non-small-cell lung carcinoma: a prospective study. J. Natl. Cancer Inst. *89*, 881–886.
2. Bielenberg, D.R., and Zetter, B.R. (2015). The contribution of angiogenesis to the process of metastasis. Cancer J. *21*, 267–273.
3. Rajabi, M., and Mousa, S.A. (2017). The role of angiogenesis in cancer treatment. Biomedicines *5*, 34.
4. Hoeben, A., Landuyt, B., Highley, M.S., Wildiers, H., Van Oosterom, A.T., and De Bruijn, E.A. (2004). Vascular endothelial growth factor and angiogenesis. Pharmacol. Rev. *56*, 549–580.
5. Potente, M., Ghaeni, L., Baldessari, D., Mostoslavsky, R., Rossig, L., Dequiedt, F., Haendeler, J., Mione, M., Dejana, E., Alt, F.W., et al. (2007). SIRT1 controls endothelial angiogenic functions during vascular growth. Genes Dev. *21*, 2644–2658.
6. Vasko, R., Xavier, S., Chen, J., Lin, C.H., Ratliff, B., Rabadi, M., Maizel, J., Tanokuchi, R., Zhang, F., Cao, J., and Goligorsky, M.S. (2014). Endothelial sirtuin 1 deficiency perpetrates nephrosclerosis through downregulation of matrix metalloproteinase-14: relevance to fibrosis of vascular senescence. J. Am. Soc. Nephrol. *25*, 276–291.
7. Pillai, V.B., Sundaresan, N.R., and Gupta, M.P. (2014). Regulation of Akt signaling by sirtuins: its implication in cardiac hypertrophy and aging. Circ. Res. *114*, 368–378.
8. Wang, R.H., Kim, H.S., Xiao, C., Xu, X., Gavrilova, O., and Deng, C.X. (2011). Hepatic Sirt1 deficiency in mice impairs mTorc2/Akt signaling and results in hyperglycemia, oxidative damage, and insulin resistance. J. Clin. Invest. *121*, 4477–4490.
9. Sayed, D., and Abdellatif, M. (2011). MicroRNAs in development and disease. Physiol. Rev. *91*, 827–887.
10. Huang, S.C., Wang, M., Wu, W.B., Wang, R., Cui, J., Li, W., Li, Z.L., Li, W., and Wang, S.M. (2017). miR-22-3p inhibits arterial smooth muscle cell proliferation and migration and neointimal hyperplasia by targeting HMGB1 in arteriosclerosis obliterans. Cell Physiol. Biochem. *42*, 2492–2506.
11. Xiong, J. (2012). Emerging roles of microRNA-22 in human disease and normal physiology. Curr. Mol. Med. *12*, 247–258.
12. Heusschen, R., van Gink, M., Griffioen, A.W., and Thijssen, V.L. (2010). MicroRNAs in the tumor endothelium: novel controls on the angioregulatory switchboard. Biochim. Biophys. Acta *1805*, 87–96.
13. Fukuyama, T., Ichiki, Y., Yamada, S., Shigematsu, Y., Baba, T., Nagata, Y., Mizukami, M., Sugaya, M., Takenoyama, M., Hanagiri, T., et al. (2007). Cytokine production of lung cancer cell lines: correlation between their production and the inflammatory/immunological responses both in vivo and in vitro. Cancer Sci. *98*, 1048–1054.

14. Desai, S., Kumar, A., Laskar, S., and Pandey, B.N. (2013). Cytokine profile of conditioned medium from human tumor cell lines after acute and fractionated doses of gamma radiation and its effect on survival of bystander tumor cells. Cytokine *61*, 54–62.

15. Püschel, F., Favaro, F., Redondo-Pedraza, J., Lucendo, E., Iurlaro, R., Marchetti, S., Majem, B., Eldering, E., Nadal, E., Ricci, J.E., et al. (2020). Starvation and antimetabolic therapy promote cytokine release and recruitment of immune cells. Proc. Natl. Acad. Sci. USA *117*, 9932–9941.

16. Levina, V., Su, Y., Nolen, B., Liu, X., Gordin, Y., Lee, M., Lokshin, A., and Gorelik, E. (2008). Chemotherapeutic drugs and human tumor cells cytokine network. Int. J. Cancer *123*, 2031–2040.

17. Pahl, H.L. (1999). Activators and target genes of Rel/NF-kappaB transcription factors. Oncogene *18*, 6853–6866.

18. Markopoulos, G.S., Roupakia, E., Tokamani, M., Alabasi, G., Sandaltzopoulos, R., Marcu, K.B., and Kolettas, E. (2018). Roles of NF-κB signaling in the regulation of miRNAs impacting on inflammation in cancer. Biomedicines *6*, 40.

19. Eichhorn, S.W., Guo, H., McGeary, S.E., Rodriguez-Mias, R.A., Shin, C., Baek, D., Hsu, S.H., Ghoshal, K., Villén, J., and Bartel, D.P. (2014). mRNA destabilization is the dominant effect of mammalian microRNAs by the time substantial repression ensues. Mol. Cell *56*, 104–115.

20. Hu, Y., Liu, H.X., Jena, P.K., Sheng, L., Ali, M.R., and Wan, Y.Y. (2020). *miR-22* inhibition reduces hepatic steatosis via FGF21 and FGFR1 induction. JHEP Rep *2*, 100093.

21. Presta, M., Dell'Era, P., Mitola, S., Moroni, E., Ronca, R., and Rusnati, M. (2005). Fibroblast growth factor/fibroblast growth factor receptor system in angiogenesis. Cytokine Growth Factor Rev. *16*, 159–178.

22. Gu, Y., Becker, V., Zhao, Y., Menger, M.D., and Laschke, M.W. (2019). miR-370 inhibits the angiogenic activity of endothelial cells by targeting smoothened (SMO) and bone morphogenetic protein (BMP)-2. FASEB J. *33*, 7213–7224.

23. Zheng, Y., and Xu, Z. (2014). MicroRNA-22 induces endothelial progenitor cell senescence by targeting AKT3. Cell Physiol. Biochem. *34*, 1547–1555.

24. Gu, W., Zhan, H., Zhou, X.Y., Yao, L., Yan, M., Chen, A., Liu, J., Ren, X., Zhang, X., Liu, J.X., and Liu, G. (2017). MicroRNA-22 regulates inflammation and angiogenesis via targeting VE-cadherin. FEBS Lett. *591*, 513–526.

25. Siegel, R.L., Miller, K.D., and Jemal, A. (2020). Cancer statistics, 2020. CA Cancer J. Clin. *70*, 7–30.

26. Zappa, C., and Mousa, S.A. (2016). Non-small cell lung cancer: current treatment and future advances. Transl. Lung Cancer Res. *5*, 288–300.

27. Würdinger, T., Tannous, B.A., Saydam, O., Skog, J., Grau, S., Soutschek, J., Weissleder, R., Breakefield, X.O., and Krichevsky, A.M. (2008). miR-296 regulates growth factor receptor overexpression in angiogenic endothelial cells. Cancer Cell *14*, 382–393.

28. Lopes-Bastos, B.M., Jiang, W.G., and Cai, J. (2016). Tumour-endothelial cell communications: important and indispensable mediators of tumour angiogenesis. Anticancer Res. *36*, 1119–1126.

29. Voronov, E., Carmi, Y., and Apte, R.N. (2014). The role IL-1 in tumor-mediated angiogenesis. Front. Physiol. *5*, 114.

30. Wang, B., Li, D., Filkowski, J., Rodriguez-Juarez, R., Storozynsky, Q., Malach, M., Carpenter, E., and Kovalchuk, O. (2018). A dual role of miR-22 modulated by RelA/p65 in resensitizing fulvestrant-resistant breast cancer cells to fulvestrant by targeting FOXP1 and HDAC4 and constitutive acetylation of p53 at Lys382. Oncogenesis *7*, 54.

31. O'Brien, J., Hayder, H., Zayed, Y., and Peng, C. (2018). Overview of microRNA biogenesis, mechanisms of actions, and circulation. Front. Endocrinol. (Lausanne) *9*, 402.

32. Valinezhad Orang, A., Safaralizadeh, R., and Kazemzadeh-Bavili, M. (2014). Mechanisms of miRNA-mediated gene regulation from common downregulation to mRNA-specific upregulation. Int. J. Genomics *2014*, 970607.

33. Segal, M., and Slack, F.J. (2020). Challenges identifying efficacious miRNA therapeutics for cancer. Expert Opin. Drug Discov. *15*, 987–992.

34. Gu, Y., Ampofo, E., Menger, M.D., and Laschke, M.W. (2017). miR-191 suppresses angiogenesis by activation of NF-κB signaling. FASEB J. *31*, 3321–3333.

35. Gu, Y., Scheuer, C., Feng, D., Menger, M.D., and Laschke, M.W. (2013). Inhibition of angiogenesis: a novel antitumor mechanism of the herbal compound arctigenin. Anticancer Drugs *24*, 781–791.

36. Tomayko, M.M., and Reynolds, C.P. (1989). Determination of subcutaneous tumor size in athymic (nude) mice. Cancer Chemother. Pharmacol. *24*, 148–154.

37. Jiang, X., Hu, C., Arnovitz, S., Bugno, J., Yu, M., Zuo, Z., Chen, P., Huang, H., Ulrich, B., Gurbuxani, S., et al. (2016). miR-22 has a potent anti-tumour role with therapeutic potential in acute myeloid leukaemia. Nat. Commun. *7*, 11452.